ADVANCED OPTICAL MATERIALS
www.advopticalmat.de

Dynamically Tunable Broadband Infrared Anomalous Refraction Based on Graphene Metasurfaces

Hua Cheng, Shuqi Chen, Ping Yu, Wenwei Liu, Zhancheng Li, Jianxiong Li, Boyang Xie, and Jianguo Tian**

Metasurfaces, which are capable of generating structure and wavelength dependent phase shift, have emerged as promising means for controlling the wavefront of electromagnetic waves. Finding new ways to realize broadband frequency response as well as maintaining high conversion efficiency still requires research efforts. For the design of plasmonic metasurfaces, graphene represents an attractive alternative to metals due to its strong field confinement and versatile tunability. Here, a novel metasurface based on graphene is proposed to control the wavefront of light. Dynamically tunable anomalous refraction composed of periodically patterned graphene nanocrosses for circularly polarized waves is achieved in the infrared regime. Broadband properties of anomalous refraction are demonstrated by investigating different frequencies and incident angles. Moreover, the anomalous conversion efficiency can be dynamically tuned and remain as high in a broadband frequency range by varying the Fermi energy without reoptimizing the nanostructures. This work may offer a further step in the development of a tunable wavefront controlling device.

1. Introduction

Optical metasurfaces have attracted more and more attention, since they are promising for novel device applications, such as anomalous refraction,[1–3] ultrathin flat lens,[4,5] surface plasmon couplers,[6,7] holograms,[8–12] vortex beam generation[13–15] and broadband quarter wave plates.[16] Realization of anomalous refraction is the basic topic among these applications by carefully engineering the parameters of structures to cover the phase range from 0 to 2π while maintaining uniform scattering amplitude. Generally, both the phase shift and the scattering amplitude are intrinsically structure and wavelength dependent, which can be hardly maintained. Recently, anomalous refractions with equal amplitude of scattering light are achieved easily by circular polarization based on metasurfaces.[14] The phase shift is dispersionless, independent of spectral response or wavelength of incident light. However, the anomalous refraction efficiency is closely related to the resonance. The highest anomalous refraction efficiency will occur at the resonant wavelength, and decrease when the wavelength of incident light is away from it. The highest conversion efficiency has to be tuned to different wavebands by carefully reoptimizing and resizing the geometric parameters of the structures. This lacks flexibility for active control, which limits its uses in practice.

One way to realize the active control of the anomalous refraction efficiency may be integrating metasurfaces with permittivity-tunable materials.[17–19] By external stimulus such as electric and/or magnetic field, voltage, or temperature, the optical response of the integrated metasurfaces can be actively controlled. Graphene, which is a single 2D plane of carbon atoms arranged in a honeycomb lattice, has been demonstrated to support surface plasmon polaritons.[20,21] As its conductivity can be dynamically controlled by electrostatic gating, it seems to be a good candidate for designing tunable devices and becomes a hot material in both physics and engineering.[22–26] Graphene-based metamaterials have been wildly demonstrated to achieve tunable devices such as absorbers,[27] antennas,[28,29] polarization converters,[30–32] and transformation optical devices.[33] Recently, metasurfaces based on 1D graphene nanoribbons have been demonstrated to manipulate wavefront of light.[34] Since only the width of 1D nanoribbon is adjustable, the conductivity of the nanoribbons needs to be individually adjusted to realize the phase range covering from 0 to 2π, which is difficult in practical applications. However, there are more adjustable structural parameters for 2D graphene nanostructures to satisfy the phase condition. The new degrees of freedom of graphene metasurfaces may facilitate arbitrary manipulation of light wavefront by uniform conductivity and will profoundly affect a wide range of photonic applications.

Here, we propose a highly tunable broadband anomalous refraction composed of periodically patterned graphene nanocrosses for circularly polarized waves in the infrared regime. We demonstrate the applicability of the scheme to generalize anomalous refraction by investigating the effect at various incident angles and different wavelengths. More importantly, the anomalous conversion efficiency can be dynamically tuned and remain as high in a broadband frequency range by varying the

Prof. H. Cheng, Prof. S. Chen, Dr. P. Yu, Dr. W. Liu, Dr. Z. Li, Dr. J. Li, Dr. B. Xie, Prof. J. Tian
Laboratory of Weak Light Nonlinear Photonics
Ministry of Education
School of Physics and Teda Applied Physics Institute
Nankai University
Tianjin 300071, China
E-mail: schen@nankai.edu.cn; jjtian@nankai.edu.cn

DOI: 10.1002/adom.201500285

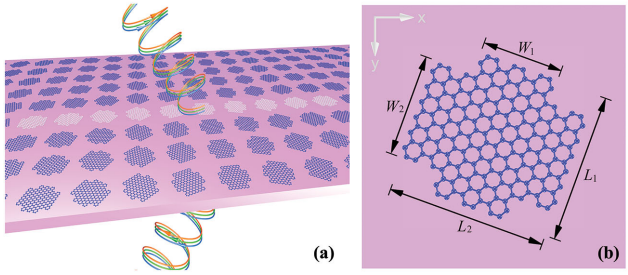

Figure 1. a) Schematic model of graphene nanocrosses metasurface. Cartesian coordinate system is applied with *z*-axis normal to the metasurface and *x*-axis along the periodically arranged direction (with one unit cell highlighted in white color). b) A single graphene nanocross of our design: L_1 = 1000 nm, L_2 = 1050 nm, $W_1 = W_2$ = 700 nm, and separation distance between each nanocross S = 2000 nm in both *x* and *y* direction. Rotation angle ϕ of graphene nanocross is defined as the angle between the length direction of one arm (along L_1) and *x* axis.

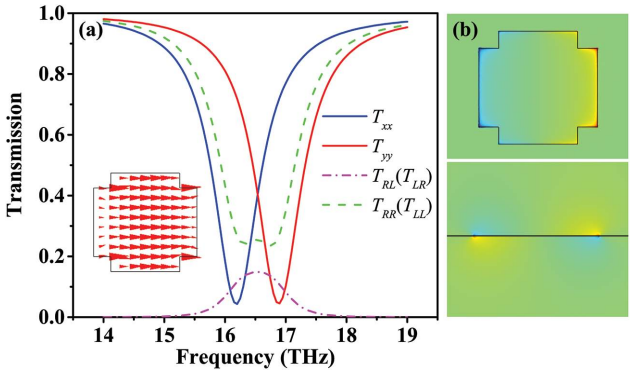

Figure 2. a) Calculated transmittance of individual graphene nanocross with rotation angle of ϕ = 90° excited by linearly polarized light and circular polarized light, respectively. The inset shows the electric displacement at the resonant frequency of 16.2 THz along the *x* direction. b) The *z*-component of electric near-field at resonant frequency of 16.2 THz along the *x* direction. The upper figure is under top view, while the lower figure is under section view.

Fermi energy without reoptimizing the nanostructures, which offers possible applications as wavefront shaping devices.

2. Results and Discussion

The designed anomalous refraction device based on graphene metasurfaces is shown in **Figure 1**a. One unit cell of the graphene metasurface comprises ten graphene nanocrosses with the same geometry, but linearly varied orientations with a step size of $\pi/10$ along the *x*-direction. The separation distance between each nanocross is of S = 2000 nm in both *x* and *y* direction, thus it repeats with a periodicity of 20 μm in the *x* direction and 2 μm in the *y* direction. The conductivity of graphene σ is computed within the local random phase approximation limit at room temperature[35]

$$\sigma(\omega)=\frac{2e^2T}{\pi\hbar^2}\frac{i}{\omega+i\tau^{-1}}\log\left[2\cosh\left(\frac{E_F}{2k_BT}\right)\right]+\frac{e^2}{4\hbar}\left[H\left(\frac{\omega}{2}\right)+\frac{4i\omega}{\pi}\int_0^\infty\frac{H(\varepsilon)-H(\omega/2)}{\omega^2-4\varepsilon^2}\right] \quad (1)$$

where $H(\varepsilon)=\sinh\left[\hbar\varepsilon/(k_BT)\right]/\left\{\cosh\left[E_F/(k_BT)\right]+\cosh\left[\hbar\varepsilon/(k_BT)\right]\right\}$. The intrinsic relaxation time is expressed as $\tau=\mu E_F/ev_F^2$, where $v_F\approx c/300$ is the Fermi velocity and $\mu=10\,000\,\mathrm{cm^2\,Vs^{-1}}$ is the measured DC mobility.[36] The finite element method (FEM) based software of COMSOL Multiphysics[37] was used to design and optimize the graphene metasurfaces. A left handed circularly polarized (LCP) or right handed circularly polarized (RCP) plane wave with an incident angle θ is used as the excitation source, and floquet periodic boundary conditions in all *x*-*z* and *y*-*z* planes are considered. The incident angle θ is defined as the angle between the wavevector and the *z*-axis of the coordinate.

Let us first consider the illumination of two normally orthogonal polarizations to directly demonstrate excitation of surface plasmons in free-standing graphene. The transmission coefficients of *x*-polarized, *y*-polarized, LCP or RCP transmitted waves are defined as $T_{ij}=\left|E_j^{\mathrm{Trans}}/E_i^{\mathrm{Inc}}\right|(i,j=x,y,L,R)$, where E_i^{Inc} and E_j^{Trans} are the electric field of the *x*-polarized, *y*-polarized, LCP or RCP incident and transmitted wave, respectively. The transmission spectra of a single graphene nanocross (with rotation angle of ϕ = 90°) are shown in **Figure 2**a, which show two distinct resonant peaks at 16.2 THz along the *x* direction and 16.9 THz along the *y* direction, when the Fermi energy is 0.95 eV. The transmission coefficient of T_{RL} (T_{LR}) reaches maximum at the intersected frequency of T_{xx} and T_{yy}, indicating the highest conversion efficiency of its cross polarized light. To further understand the nature of these resonances, the electric displacement and *z*-component electric near-field at resonant frequency of 16.2 THz along the *x* direction are calculated and demonstrated in the inset of Figure 2a,b. The upper figure is under top view, while the lower is under section view. As it is shown, efficient electric dipole mode is excited at the resonant frequency.[38] The strong resonances demonstrate very efficient excitation of surface plasmons in graphene. Surface plasmon excitations in graphene nanocross correspond to collective oscillations of electrons across each length of nanobars (L_2, L_1), where plasmon frequency scales with different bar length. The origin of the resonances can be interpreted as the electric dipole modes coupled to propagating light.

Optical antennas with equal scattering amplitudes and phase coverage over the whole 0 to 2π are necessary for designing anomalous refraction. Following the approach previously discussed,[1] the generalized Snell's law for anomalous refraction can be expressed as

$$n_t\sin\theta_t-n_i\sin\theta_i=\frac{\lambda_0}{2\pi}\frac{d\Phi}{dx}=\sigma\frac{\lambda_0}{S}, \quad (2)$$

where $d\Phi/dx$ refers to phase gradient along the surface, and $\sigma=\pm1$ correspond to the helicity of RCP and LCP incident light. θ_i *and* θ_t are incident and refracted angles, respectively. Equation (2) apparently shows that the refractive angle can be tuned by controlling the phase shift or frequency at plasmonic metasurface. The phase shift of the scattered circularly polarized light with opposite handedness is determined solely by the orientation of the dipole[14]

Adv. Optical Mater. **2015**,
DOI: 10.1002/adom.201500285

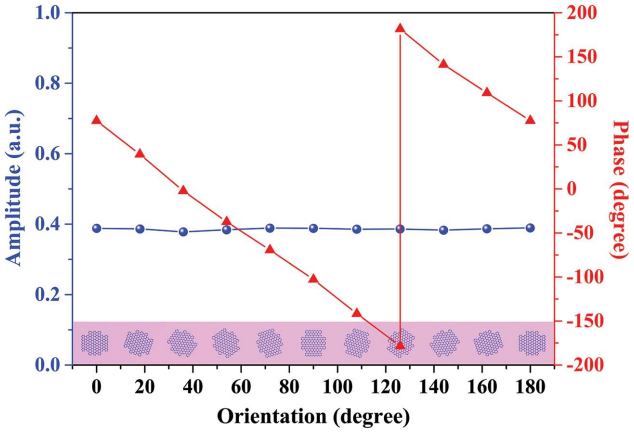

Figure 3. Calculated transmission amplitude and phase profile of the anomalous light along the graphene nanocross array.

$$E_{rad} \propto \left[\frac{\cos\theta\cos\xi+1}{4} E_u^{\sigma} + \frac{(\cos\theta+1)(\cos\xi+1)+1}{8} E_u^{-\sigma} e^{+\sigma i 2\varphi} \right], \quad (3)$$

where θ and ξ are the incident and observation angle. The scattered light with opposite handedness polarization has a phase change of $2\sigma\varphi$, where φ is the rotation angle of the graphene nanocross. In our simulation, we choose ten graphene nanocrosses that scatter circular polarized light into opposite handedness polarization with constant amplitudes and an incremental phase of $\pi/5$ between neighbors. **Figure 3** shows the opposite handedness polarized transmission amplitudes and the corresponding phase shifts for an individual graphene nanocross at the frequency of 17 THz, where the Fermi enery is fixed at 0.95 eV. Obviously, each graphene nanocross with different orientations has same ability to refract light into opposite helicity, with a high amplitude conversion efficiency of about 0.4 and the entire phase range covering from 0 to 2π.

Compared with traditional plasmonic metasurfaces, the most important advantage for the graphene plasmonic metasurfaces is the capability of dynamically tuning the conductivity through chemical or electrostatic gating. To demonstrate the tunability of the anomalous refraction, we calculated the amplitude of anomalous refraction of LCP as a function of Fermi energy and frequency in **Figure 4**a. Pentagrams in the figure denote the maximum amplitudes of anomalous refraction. As the Fermi energy increases from 0.75 to 1 eV, the maximum anomalous conversion efficiency, which corresponds to the amplitude of anomalous refraction (pentagrams in Figure 4a), will shift to higher frequencies. Figure 4b gives the amplitude of anomalous refraction versus frequency for the Fermi energy of 0.95 eV. For a fixed Fermi energy, the highest anomalous conversion efficiency occurs at the intersected frequency of the two resonances along x and y directions. It will decrease when the frequency is away from the intersected frequency. Meanwhile, the amplitude of anomalous refraction with respect to Fermi energy for a fixed frequency of 15.7 THz is also shown in Figure 4c, indicating its dynamic tunability by Fermi energy. To demonstrate the tunable broadband anomalous refraction with high conversion efficiency, we extracted the frequencies for equal amplitude of anomalous refraction from different Fermi energies, as shown in Figure 4d (see also the blue balls in Figure 4a). By changing the Fermi energy from 0.75 to 1 eV, the anomalous conversion efficiency can always be maintained at about 0.4 within a wide frequency range from 14.5 to 17 THz. Thus, the high conversion efficiency can be achieved only by tuning the Fermi energy of graphene, without changing the structure parameters.

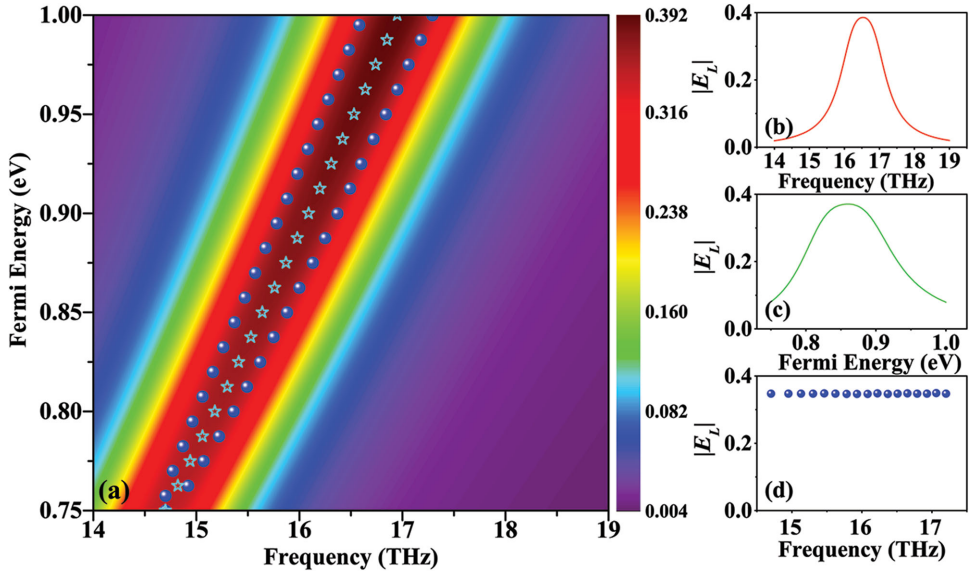

Figure 4. a) Amplitude of anomalous refraction of LCP wave as a function of Fermi energy and frequency, at normal incidence of RCP wave. The pentagrams and balls indicate the maximum amplitude and the extracted equal amplitude of anomalous refraction, respectively. b) Amplitude of anomalous refraction versus frequency when the Fermi energy is fixed at 0.95 eV. c) Amplitude of anomalous refraction as a function of Fermi energy when the frequency is fixed at 15.7 THz. d) Equal amplitude of anomalous refraction as a function of frequency.

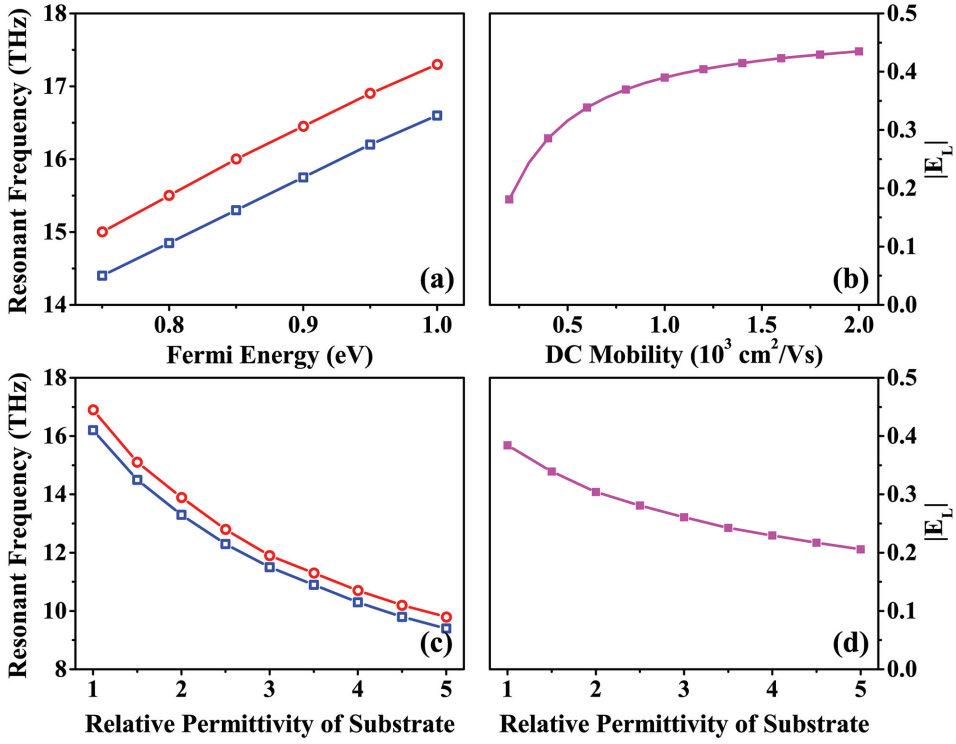

Figure 5. Calculated resonant frequencies along the two orthogonal polarizations as functions of a) Fermi energy of graphene and c) relative permittivity of substrate. Amplitude of anomalous refraction versus b) DC mobility of graphene and d) relative permittivity of substrate.

By combing the resonance condition with surface plasmon satisfied equation $k_{spp} = \hbar\omega^2/(2\alpha_0 E_F c)$,[35] the resonant frequency can be approximately expressed as $f_R \propto \sqrt{E_F/L_s}$, where L_s represents the resonance related structure parameter. The estimate is essentially consistent with the calculated resonant frequencies with different Fermi energies shown in **Figure 5**a. It shows that the resonant frequency can be tuned by changing the Fermi energy instead of the structure parameter, which makes graphene metasurfaces more repeat useful than metallic ones. It should be noted that the DC mobility of graphene film always ranges from about 1000 $cm^2\ Vs^{-1}$ (chemical vapor deposition grown graphene) to 230 000 $cm^2\ Vs^{-1}$ (suspended exfoliated graphene). We calculated the amplitude of anomalous refraction at the frequency of 17 THz as a function of DC mobility of graphene in Figure 5b. The device efficiency can be further improved by increasing of the DC mobility. Furthermore, the plasmon resonances and the amplitude of anomalous refraction of nanostructures can be strongly influenced by different kinds of substrates. We calculated the resonant frequencies and the corresponding maximum amplitude of anomalous refraction of the graphene nanocross with Fermi energy of 0.95 eV supported on substrates with different dielectric permittivities, as shown in Figure 5c,d. As the dielectric permittivity of substrate increases, the resonant peaks along the two orthogonal polarizations will have a red shift, which is consistent with that discribed by Fan et al.[25] However, the corresponding maximum amplitude of anomalous refraction will decrease.

Finally, for experimental feasibility, we simulate graphene metasurfaces on a substrate with refractive index of 1.4, which may be considered as an infrared transparent material such as potassium bromide, calcium fluoride or magnesium fluoride in experiment. The anomalous phase distributions in the *x*-*z* plane in **Figure 6**, where a constant phase gradient is created along the *x*-direction of the graphene metasurface and the incident plane waves are circularly polarized with opposite handedness polarization. The white and pink arrows indicate the directions of the incident circularly polarized light and the anomalous refracted light, respectively. The phase accumulation of the refracted beam with a propagation distance along the *z* direction can be expressed as $\Delta\varphi = k(z_2 - z_1)\cos\theta$, where θ is the refractive angle (the angle between the wavevector and *z* direction). To determine the direction of the refractive beam (refractive angle), we extracted the phase of electric field at two points (x_1, y_1, z_1) and (x_1, y_1, z_2), and then calculated the refractive angle by $\theta = \cos^{-1}\{2\pi(\varphi_2 - \varphi_1)/[\lambda(z_2 - z_1)]\}$, where φ_2 and φ_1 represent the phases at the points of (x_1, y_1, z_1) and (x_1, y_1, z_2). Figure 6a,b shows the distinct anomalous refraction phenomena for normally incident LCP light at two different frequencies of 14 and 16 THz with simulated anomalous refractive angles of 49.0° and 42.8°, respectively. By changing the helicity of the incident light to RCP, the direction of the anomalous refracted beam is switched to the other side with anomalous refractive angles of 49.1° and 42.9°, which is shown in Figure 6c,d. Oblique incidence with incident angles of 10° and 30° are also carried out for LCP light at 14 THz, as shown in Figures 6e,f, which show obvious anomalous refraction behaviors. The simulated anomalous refractive angles are 39.9° and 23.9°, respectively. Our simulated anomalous refractive angles by FEM are basically accordant with the expected

Adv. Optical Mater. **2015**,
DOI: 10.1002/adom.201500285

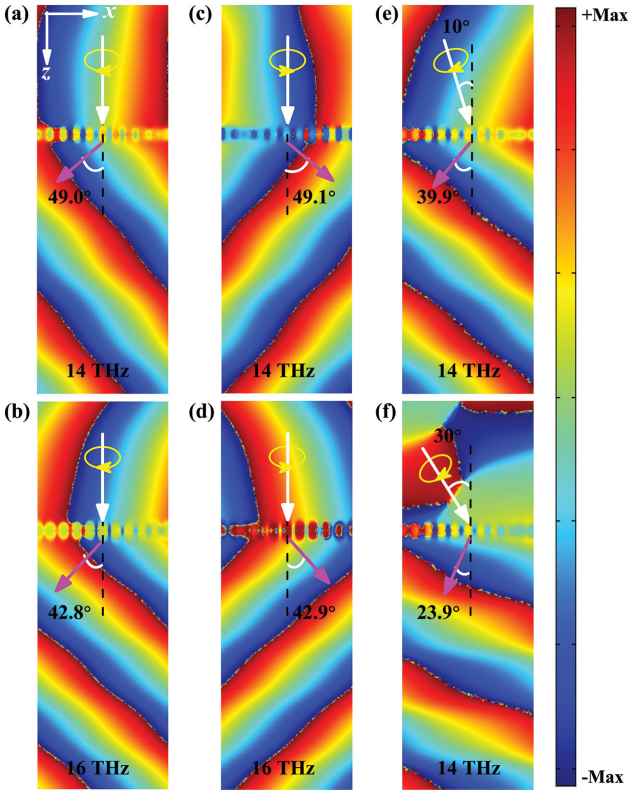

Figure 6. Simulated anomalous phase distributions of opposite handedness circular polarization when the Fermi energy is fixed at 0.95 eV. a,b) Phase distributions for two different frequencies of 14 and 16 THz at normal incidence of LCP wave. c,d) Phase distributions by change the handedness of incident wave to RCP at normal incidence, corresponding to (a, b). e,f) Phase distributions by fixing the incident frequency of 14 THz, but changing the oblique incidence angles with $\theta = 10°$ and 30°.

results calculated by Equation (2), with slight deviations due to the simulation error.

3. Conclusion

In summary, we have proposed a highly tunable anomalous refraction based on graphene metasurfaces for circularly polarized waves in the infrared regime. The anomalous refraction is demonstrated in a broadband range of frequencies and incident angles. The anomalous refraction can also occur when the polarization of the incident light is reversed. Moreover, the anomalous conversion efficiency can be dynamically tuned and remain as high in a broadband frequency range by varying the Fermi energy without reoptimizing the nanostructures to adjust the resonant frequency. This concept could not be directly extended to optical or near infrared regions by simply downsizing geometries, because graphene suffers from relatively weak plasmonic response and non-negligible loss in high frequencies. However, utilizing the strong plasmonic response of metal and Fermi energy variability of graphene, tunable anomalous refraction may be realized by the combination of metallic nanostructures and graphene in optical and near infrared regions. We believe the graphene plamonic metasurfaces demonstrated here may lead to practical applications for active wavefront control, such as polarization and spectral beam splitters, light absorber, and so forth.

Acknowledgements

This work was supported by the National Basic Research Program (973 Program) of China (2012CB921900), the Chinese National Key Basic Research Special Fund (2011CB922003), the Natural Science Foundation of China (61378006 and 11304163), the Program for New Century Excellent Talents in University (NCET-13–0294), the Natural Science Foundation of Tianjin (13JCQNJC01900), the Specialized Research Fund for the Doctoral Program of Higher Education (20120031120032), and the 111 project (B07013).

Received: May 25, 2015
Revised: July 28, 2015
Published online:

[1] N. Yu, P. Genevet, M. A. Kats, F. Aieta, J. Tetienne, F. Capasso, Z. Gaburro, *Science* **2011**, *334*, 333.
[2] X. Ni, N. K. Emani, A. V. Kildishev, A. BOltasseva, V. M. Shalaev, *Science* **2012**, *335*, 427.
[3] J. Li, S. Chen, H. Yang, J. Li, P. Yu, H. Cheng, C. Gu, H. T. Chen, J. Tian, *Adv. Funct. Mater.* **2015**, *25*, 704.
[4] F. Aieta, P. Genevet, M. A. Kats, N. Yu, R. Blanchard, Z. Gaburro, F. Capasso, *Nano Lett.* **2012**, *12*, 4932.
[5] X. Chen, L. Huang, H. Mühlenbernd, G. Li, B. Bai, Q. Tan, G. Jin, C. W. Qiu, S. Zhang, T. Zentgraf, *Nat. Commun.* **2012**, *3*, 1198.
[6] J. Lin, J. P. B. Mueller, Q. Wang, G. Yuan, N. Antonious, X. Yuan, F. Capasso, *Science* **2013**, *340*, 331.
[7] L. Huang, X. Chen, B. Bai, Q. Tan, G. Jin, T. Zentgraf, S. Zhang, *Lights: Sci. Appl.* **2013**, *2*, 70.
[8] L. Huang, X. Chen, H. Mühlenbernd, H. Zhang, S. Chen, B. Bai, Q. Tan, G. Jin, K. W. Cheah, C. W Qiu, J. Li, T. Zentgraf, S. Zhang, *Nat. Commun.* **2013**, *4*, 2808.
[9] F. Zhou, Y. Liu, W. Cai, *Opt. Express* **2013**, *21*, 4348.
[10] W. T. Chen, K. Yang, C. Wang, Y. Huang, G. Sun, I. Chiang, C. Y. Liao, W. Hsu, H. T. Lin, S. Sun, L. Zhou, A. Q. Liu, D. P. Tsai, *Nano Lett.* **2014**, *14*, 225.
[11] X. Ni, A. V. Kildishev, V. M. Shalaev, *Nat. Commun.* **2013**, *4*, 2807.
[12] J. Lin, P. Genevent, M. A. Kats, N. Antoniou, F. Capasso, *Nano Lett.* **2013**, *13*, 4269.
[13] P. Genevet, N. Yu, F. Aieta, J. Lin, M. A. Kats, R. Blanchard, M. O. Scully, Z. Gaburro, F. Capasso, *Appl. Phys. Lett.* **2012**, *100*, 013101.
[14] L. Huang, X. Chen, H. Mühlenbernd, G. Li, B. Bai, Q. Tan, G. Jin, T. Zentgraf, S. Zhang, *Nano Lett.* **2012**, *12*, 5750.
[15] P. Yu, S. Chen, J. Li, H. Cheng, Z. Li, W. Liu, B. Xie, Z. Liu, J. Tian, *Opt. Lett.* **2015**, *40*, 3229.
[16] N. Yu, F. Aieta, P. Genevet, M. A. Kats, Z. Gaburro, F. Capasso, *Nano Lett.* **2012**, *12*, 6328.
[17] S. Khatua, W. Chang, P. Swanglap, J. Olson, S. Link, *Nano Lett.* **2011**, *11*, 3797.
[18] N. Shen, M. Massaouti, M. Gokkavas, J. Manceau, E. Ozbay, M. Kafesaki, T. Koschny, S. Tzortzakis, C. M. Soukoulis, *Phys. Rev. Lett.* **2011**, *106*, 037403.
[19] A. A. Zharov, I. V. Shadrivov, Y. S. Kivshar, *Phys. Rev. Lett.* **2003**, *91*, 037401.
[20] F. H. L. Koppens, D. E. Chang, F. J. Javier García de Abajo, *Nano Lett.* **2011**, *11*, 3370.

[21] L. Ju, B. Geng, J. Horng, C. Girit, M. Martin, Z. Hao, H. A. Bechtel, X. Liang, A. Zettl, Y. R. Shen, F. Wang, *Nat. Nanotechnol.* **2011**, *6*, 630.
[22] S. Thongrattanasiri, F. H. L. Koppens, F. Javier García de Abajo, *Phys. Rev. Lett.* **2012**, *108*, 047401.
[23] C. Chen, C. Park, B. W. Boudouris, J. Horng, B. Geng, C. Girit, A. Zettl, M. F. Crommie, R. A. Segalman, S. G. Louie, F. Wang, *Nature* **2011**, *471*, 617.
[24] Z. Zeng, X. Huang, Z. Yin, H. Li, Y. Chen, H. Li, Q. Zhang, J. Ma, F. Boey, H. Zhang, *Adv. Mater.* **2012**, *24*, 4138.
[25] Y. Fan, N. Shen, T. Koschny, C. M. Soukoulis, *ACS Photonics* **2015**, *2*, 151.
[26] J. Zheng, L. Yu, S. He, D. Dai, *Sci. Rep.* **2015**, *5*, 7987.
[27] S. Thongrattanasiri, F. H. L. Koppens, F. Javier García de Abajo, *Phys. Rev. Lett.* **2012**, *108*, 047401.
[28] Z. Fang, S. Thongrattanasiri, A. Schlather, Z. Liu, L. Ma, Y. Wang, P. M. Ajayan, P. Nordlander, N. J. Halas, F. Javier García de Abajo, *ACS Nano* **2013**, *7*, 2388.
[29] H. Cheng, S. Chen, Y. Ping, X. Duan, B. Xie, J. Tian, *Appl. Phys. Lett.* **2013**, *103*, 203112.
[30] A. Fallahi, J. Perruisseau-Carrier, *Phys. Rev. B* **2012**, *86*, 195408.
[31] H. Cheng, S. Chen, P. Yu, J. Li, L. Deng, J. Tian, *Opt. Lett.* **2013**, *38*, 1567.
[32] H. Cheng, S. Chen, P. Yu, J. Li, B. Xie, Z. Li, J. Tian, *Appl. Phys. Lett.* **2013**, *103*, 223102.
[33] A. Vakil, N. Engheta, *Science* **2011**, *332*, 1291.
[34] F. Lu, B. Liu, S. Shen, *Adv. Opt. Mater.* **2014**, *2*, 794.
[35] F. H. L. Koppens, D. E. Chang, F. Javier García de Abajo, *Nano Lett.* **2011**, *11*, 3370.
[36] K. S. Novoselov, A. K. Geim, S. V. Morozov, D. Jiang, Y. Zhang, S. V. Dubonos, I. V. Grigorieva, A. A. Firsov, *Science* **2004**, *306*, 666.
[37] COMSOL Multiphysics User's Guide, Version 3.5 (Comsol AB, Brulington, MA, 2008).
[38] Y. Fan, Z. Wei, Z. Zhang, H. Li, *Opt. Lett.* **2013**, *38*, 5410.

Adv. Optical Mater. **2015**,
DOI: 10.1002/adom.201500285